# Plasmon-enhanced single-molecule enzymology

ACS Photonics

Article

Cite This: ACS Photonics 2018, 5, 3073−3081

# Plasmon-Enhanced Single-Molecule Enzymology

Yuyang Wang and Peter Zijlstra*

Molecular Biosensing for Medical Diagnostics, Faculty of Applied Physics, and Institute for Complex Molecular Systems, Eindhoven University of Technology, PO Box 513, 5600 MB, Eindhoven, The Netherlands

Supporting Information

**ABSTRACT:** We present a numerical study on plasmon-enhanced single-molecule enzymology. We combine Brownian dynamics and electromagnetic simulations to calculate the enhancement of fluorescence signals of fluorogenic substrate converted by an enzyme conjugated to a plasmonic particle. We simulate the Brownian motion of a fluorescent product away from the active site of the enzyme, and calculate the photon detection rate taking into account modifications of the excitation and emission processes by coupling to the plasmon. We show that plasmon enhancement can boost the signal-to-noise ratio (SNR) of single turnovers by up to 100 fold compared to confocal microscopy. This enhancement factor is a trade-off between the reduced residence time in the near-field of the particle, and the enhanced emission intensity due to coupling to the plasmon. The enhancement depends on the size, shape and material of the particle and the photophysical properties of the fluorescent product. Our study provides guidelines on how to enhance the SNR of single-molecule enzyme studies and may aid in further understanding and quantifying static and dynamic heterogeneity.

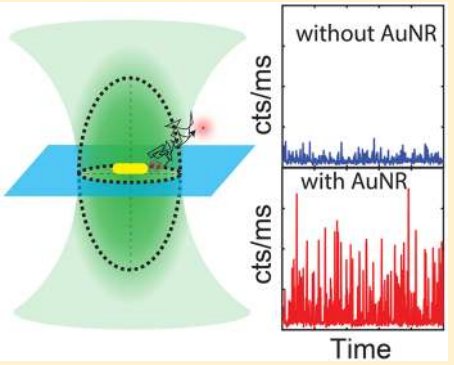


**KEYWORDS:** *Plasmonic nanoantennas, single-molecule enzymology, plasmon-enhanced fluorescence, numerical modeling, gold nanorods, Brownian motion*



Enzymes are vital biomolecules that catalyze thousands of biochemical reactions.[1] The study of enzyme kinetics started with the work of Michaelis and Menten,[2] which plays an essential role in analyzing the kinetics of an ensemble of enzymes. Such ensemble studies assume that all enzymes in solution are identical; however, recent single-molecule studies revealed that the catalytic rates in a population of enzymes are heterogeneous (static heterogeneity).[3,4] Furthermore, it was observed that the turnover rate of individual enzymes exhibits temporal fluctuations (dynamic heterogeneity).[5−8] It may well be that such heterogeneity has far-reaching biological consequences, slowly fluctuating enzymes are, for example, implicated in variations in antibiotic resistance of genetically identical bacteria.[9]

Single-molecule confocal microscopy has been used to record the kinetic behavior of single immobilized enzymes,[5−8,10−14] and often fluorogenic substrates are used that are converted by the enzyme from a dark to an emitting state.[15,16] The activity of the enzyme is then visualized as a series of fluorescence bursts caused by the diffusion of the fluorescent product out of the confocal volume.[16] This approach has been used to study the activity of enzymes such as cholesterol oxidase,[5] $\beta$-galactosidase,[7] chymotrypsin,[14] lipase B,[6,11] and $\lambda$-exonuclease.[12] These pioneering studies reported temporal fluctuations in activity on time scales of milliseconds to seconds, which were attributed to conformational fluctuations.[5,7,11]

However, the average signal-to-noise ratio (SNR) of these bursts ranges from 1 to 4 in practice.[13,14] The SNR is limited by the fluorescent background caused by, for example, the presence of a small fraction of autohydrolized product in the large confocal volume. In addition, the SNR of individual bursts is broadly distributed around its mean since each fluorescent product diffuses out of the confocal volume through a random path determined by Brownian motion. This complicates the interpretation of single-enzyme data and the quantification of the degree of heterogeneity because a significant fraction of the bursts exhibits a SNR < 1 and is missed in the analysis.[14,15,17−19]

Recently, zero-mode waveguides (ZMW) have been used to increase the SNR in the detection of single-molecule fluorescence.[20,21] ZMWs efficiently reduce the fluorescent background from solution-phase product by confining light to zeptoliter volumes in small apertures that are milled in a metal film. Using ZMWs, single turnovers of DNA polymerase were recorded with increased SNR and higher background fluorophore concentrations.[20] However, signal enhancements are modest due to quenching by the large volume of nearby metal.[22,23] The plasmon resonance of single metal nanoparticles on the other hand provides both confinement of the excitation to zeptoliter volumes, and can additionally strongly enhance the emitted intensity because the particle acts as a nano-antenna.[24,25]

The origin of the plasmon enhancement of single-molecule fluorescence is the modification of the excitation and decay rates of a molecular dipole close to a particle. The locally

Received: March 13, 2018
Published: May 23, 2018

  

DOI: 10.1021/acsphotonics.8b00327
ACS Photonics 2018, 5, 3073−3081

enhanced field leads to a dramatic increase of the excitation rate, whereas the nanoantenna modifies the emission of the fluorophore due to modulations of the radiative and nonradiative decay rate.[26−29] Fluorescence intensity enhancements in excess of $10^3$ to $10^5$ have been reported for single gold nanorods,[30,31] metallic particles on a film,[32] lithographically fabricated nanogaps,[33] and self-assembled gold nanoparticle dimers.[34−36] Plasmonic nanoantennae have already been used to extend fluorescence correlation spectroscopy to micromolar concentations,[21,37−42] to study single light-harvesting complexes,[43] and to study diffusion of membrane-proteins.[44]

Here we propose the use of single plasmonic nanoparticles to enhance the SNR of single-molecule enzymology. We combine Brownian dynamics and electromagnetic simulations to model the number of photons generated by a single fluorescent product that diffuses away from the active site of the enzyme. The simulations account for modifications of the excitation, radiative, and nonradiative rates of the fluorophore by the presence of the nanoantenna. Our approach differs from previous ensemble-averaged approaches of plasmon-enhanced fluorescence where molecular excitation and detection functions were used to simulate fluorescence correlation spectroscopy (FCS) curves.[37,38] We explicitly simulate the trajectories of each single molecule and reconstruct the time-dependent intensity and SNR on a molecule-by-molecule basis. In contrast to fluorescence-correlation spectroscopy models, this yields information on molecule-to-molecule variations in the detected intensity and SNR. Establishing these variations is especially critical for single-molecule enzymology where no event should be missed. The Brownian dynamics simulations reveal that a fluorescent product resides in the particle's near-field 100−1000× shorter compared to a confocal excitation volume. Despite this shorter residence time the resulting SNR is increased up to 100-fold due to enhancements by the nanoantenna. We show that the SNR enhancement depends on the size, shape and material of the plasmonic particle and on the photophysical properties of the fluorescent product.

## COMPUTATIONAL APPROACH

We consider a particle−enzyme complex in the presence of a solution of fluorogenic substrate molecules, placed in a diffraction-limited confocal volume of a laser beam (Figure 1). In a typical confocal fluorescence measurement, a focused laser beam illuminates a confined volume of fluorophores that undergo Brownian motion. The enzyme converts a non-fluorescent substrate to a fluorescent product, and this generated fluorophore will follow a Brownian motion trajectory (a series of 3D coordinates as a function of time) to eventually diffuse out of the focus.

To assess the effect of the nanoantenna on the SNR we compare the SNR in the absence and the presence of the particle. We focus our analysis on spherical and rod-shaped gold particles due to their widespread use and ease of synthesis.[45] The simulation of the signal and background signals consists of the following steps:

1. Generation of Brownian motion trajectories of single product molecules that diffuse away from the active site of the enzyme. The trajectories consist of a 3D random walk with a total length of 1 ms and a given time step of 10 ns. The mean squared displacement (MSD) of the molecule derives from the Stokes−Einstein equation:

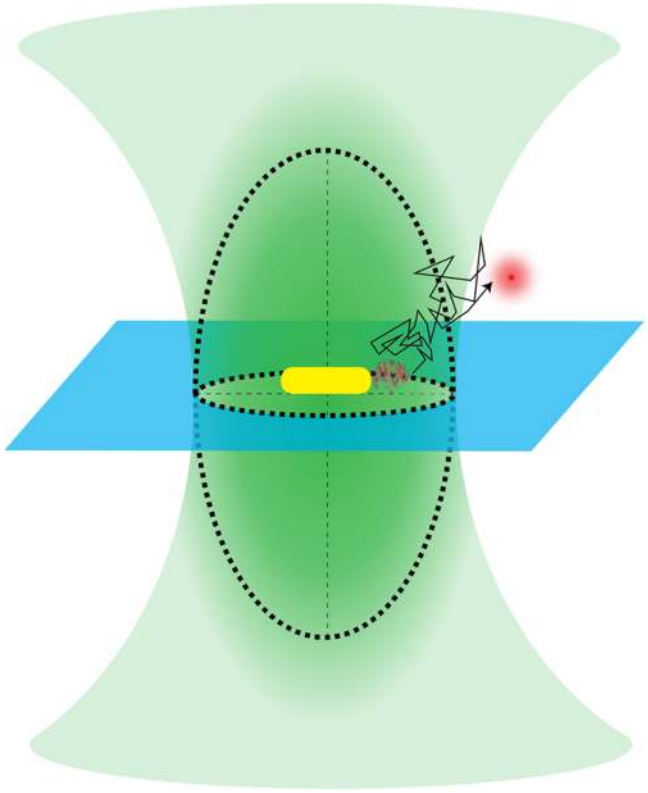

**Figure 1.** Confocal excitation of an enzyme-gold nanoparticle complex. An enzyme is coupled to a gold nanoparticle that is immobilized on a glass surface (blue) and located in the center of a confocal laser beam (green). The active site of the enzyme converts nonfluorescent substrate to an emitting product (red) that follows a Brownian motion trajectory once released from the active site.

$$D = \frac{k_B T}{6\pi\eta r} \tag{1}$$

with $D$ being the diffusion coefficient ($m^{-2}$ $s^{-1}$), $k_B$ is the Boltzmann's constant (J $K^{-1}$), $T$ is the absolute temperature (K), $\eta$ is the dynamic viscosity of water (Pa s), and $r$ is the hydrodynamic radius of the molecule (m). The MSD for 3D free diffusion is then given by (see Supporting Information, Figure S4):

$$\mathrm{MSD} = 6D\tau \tag{2}$$

2. Calculation of the position-dependent emission rate, taking into account the plasmon-induced modifications of the excitation rate, radiative, and nonradiative decay rate of the fluorophore. The photon count rate PCR of a fluorophore can be expressed as

$$\mathrm{PCR} = \frac{\sigma_{abs}}{h\nu}\phi I_{exc} \tag{3}$$

where $I_{exc}$ is the position-dependent excitation intensity (W $m^{-2}$), $\sigma_{abs}$ is the absorption cross section of the fluorophore ($m^2$), $\phi$ is the fluorophore's quantum yield defined as $\phi = \frac{\gamma_r}{\gamma_r + \gamma_{nr}}$, with $\gamma_r$ and $\gamma_{nr}$ being the radiative and nonradiative decay rates ($s^{-1}$) and $h\nu$ the photon energy (J).

Equation 3 is valid in the weak excitation regime, in which the photon count rate of a fluorophore is linear in incident intensity. To take into account saturation effects



DOI: 10.1021/acsphotonics.8b00327
ACS Photonics 2018, 5, 3073−3081

we introduce the saturation intensity $I_{sat} = \frac{\gamma_{tot} h\nu}{2\sigma_{abs}}$ with $\gamma_{tot} = \gamma_r + \gamma_{nr}$, where we ignored triplet state dynamics.[43] This yields the following expression for the PCR of a single product (see Supporting Information):

$$PCR = \frac{\sigma_{abs}}{h\nu} \frac{\gamma_r}{\gamma_{tot}} \frac{I_{exc} I_{sat}}{I_{exc} + I_{sat}} \quad (4)$$

In the absence of a nanoparticle, the only position-dependent term in the above equations is $I_{exc}$, whose position dependence is given by the 3D Gaussian approximation of the confocal volume. The other terms are assumed position-independent. In the presence of a plasmonic particle, however, the decay rates $\gamma_r$ and $\gamma_{nr}$ will also be modified depending on the location of the fluorophore with respect to the particle. These rate-modifications are calculated numerically using the Boundary Element Method. In all simulations we used the typical photophysical parameters of a red fluorescence dye in free space: the absorption cross section $\sigma_{abs}$ of $10^{-20}$ m$^2$, the fluorescence lifetime $\tau_{lifetime}$ of 10 ns, and corresponding total decay rate $\gamma_{tot}$ of $10^8$ s$^{-1}$.

3. Calculation of the background signal $PCR_{bg}$ for a certain fraction of autohydrolized substrate using eq 4, but without plasmon-enhancement. Herein we ignore the possible background and noise from autohydrolyzed product diffusing through the plasmon-enhanced near field because the near field is >$10^4$× smaller than the confocal volume. We then find $PCR_{bg}$ by

$$PCR_{bg} = n_A c_{subs} V_{conf} f_h \cdot PCR \quad (5)$$

where here the PCR for a fluorophore in the center of a 3D Gaussian beam is used, $n_A$ is Avogadro's constant, $c_{subs}$ is the substrate concentration (M), $V_{conf}$ is the confocal volume (L), and $f_h$ is the fraction of autohydrolyzed substrate. In order to acquire a realistic signal and noise level as reported in existing experimental work for the confocal-only case,[7] we set $f_h$ = 0.002‰ and the collection efficiency of the setup $\eta_{col}$ = 6%.

We then calculate the PCR of single diffusing products for each position of the fluorophore in the Brownian trajectory, yielding the time-dependent PCR($\tau$). Time traces of multiple subsequent turnovers are generated by randomly assigning a time stamp to every turnover and stitching the corresponding PCR($\tau$). The average frequency of events was set to 400 Hz to match the typical turnover rate of an enzyme with reasonable activity.[1,46] We then generate the expected experimental timetrace by taking into account the collection efficiency of the setup $\eta_{col}$ and the integration time $t_{int}$. This yields the number of detected photons per integration time, $N_{det}(t)$:

$$N_{det}(t) = \int_t^{t+t_{int}} (PCR(\tau) + PCR_{bg})\eta_{col} d\tau \quad (6)$$

4. Based on the above calculations, we determine the signal-to-noise ratio (SNR) of each event by dividing the peak photon counts from a single turnover by the shotnoise originating from both the signal and background counts.

## RESULTS AND DISCUSSION

The electromagnetic field around the particle is enhanced compared to the incident illumination, resulting in an enhanced excitation rate of fluorophores located in this near field. The excitation enhancement can therefore be defined as $\xi_{exc} = \frac{I_{exc}}{I_0}$, where $I_0$ is the maximum intensity at the center of an incident 3D Gaussian excitation beam. In Figure 2a, we show the numerically calculated near field intensity around a nanorod of 82 × 30 nm$^2$, evaluated on resonance with the longitudinal plasmon at 705 nm. We observe an enhanced intensity around the two tips of the gold nanorod of nearly $\xi_{exc}$ = 1000, in good agreement with previous studies.[31] This enhancement decays

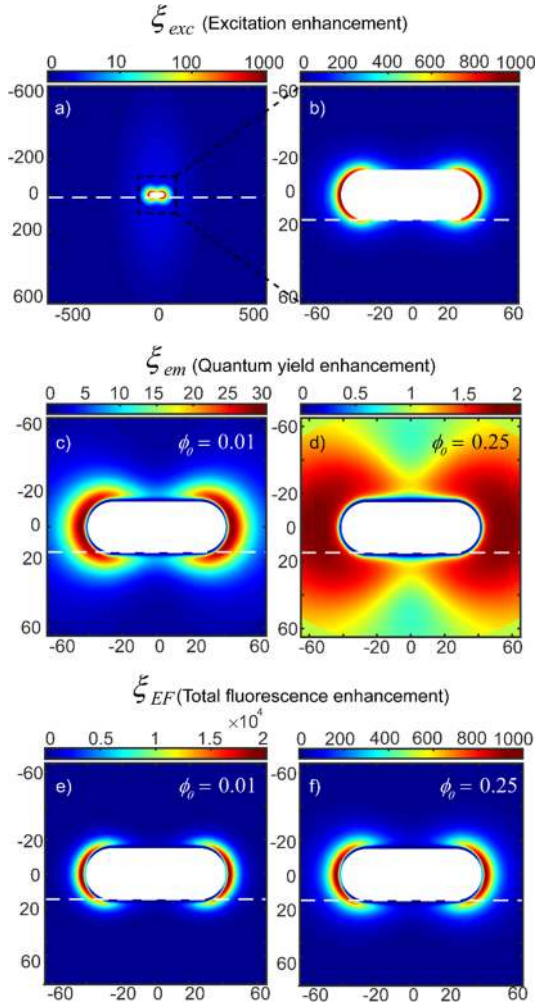


**Figure 2.** Numerical calculations of the local intensity enhancement and rate-enhancements around an 82 × 30 nm$^2$ gold nanorod. (a) Excitation enhancement shown by normalized $I_{exc}$ containing both distributions from the 3D Gaussian point-spread-function of an excitation beam with a maximum intensity of $I_0$, and the gold nanorod near field. The near field enhancement around the particle was calculated for excitation with a plane wave at 705 nm (resonant with the longitudinal plasmon). (b) Zoom of the gold nanorod in (a). (c, d) Quantum yield enhancement for a dipolar emitter with an intrinsic quantum yield $\phi_0$ of 1% and 25%, respectively (orientation averaged). The emitter is modeled by a narrow absorption line at 705 nm, with a narrow emission line with a Stokes shift of 25 nm. (e, f) Total fluorescence enhancement for excitation at 705 nm and emission at 730 nm. Note the difference in the color scale.



DOI: 10.1021/acsphotonics.8b00327
ACS Photonics 2018, 5, 3073−3081

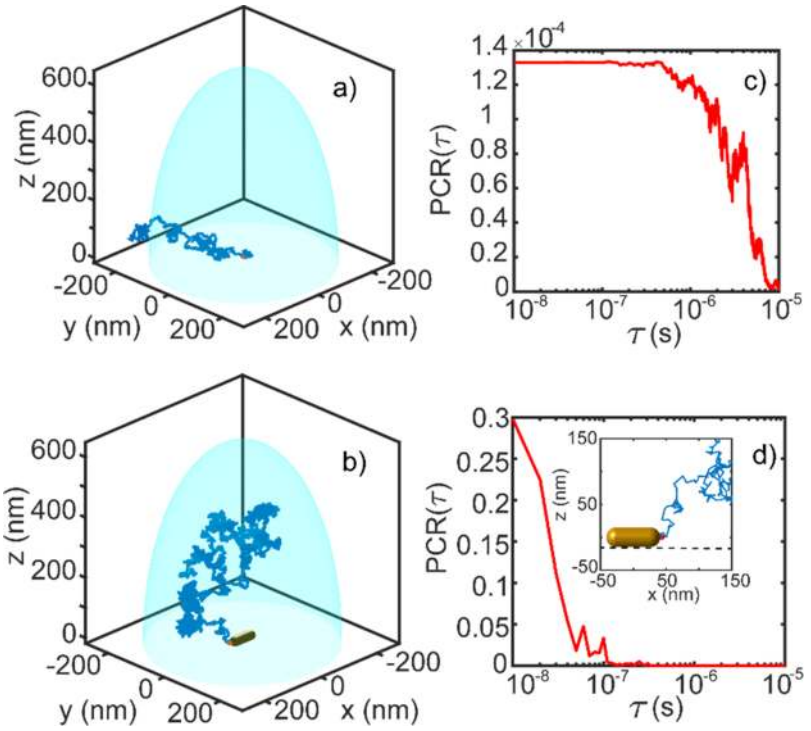


**Figure 3.** Simulated Brownian motion trajectories of a fluorophore out of a 3D Gaussian focus (a, c) without and (b, d) with a 82 × 30 nm$^2$ AuNR. The blue half-ellipses illustrate the approximate $1/e^2$ beam size of the 3D Gaussian focus. (b, d) Corresponding PCR($\tau$) as a function of time for the trajectories shown in (a) and (c). The inset in (d) shows the first few points in the trajectory projected on the $x$−$z$ plane. The dotted line in the inset illustrates the planar infinite substrate, acting as a hard boundary for the diffusion. The simulation is performed for $\phi_0$ = 25% and $I_0$ = $10^8$ W m$^{-2}$ (corresponding to a 705 nm laser with a power of 20 $\mu$W focused with an objective lens with NA = 1.2) and a time step of 10 ns in the Brownian motion calculations.

rapidly away from the particle surface on length-scales of ∼5 nm. The excitation is thus strongly confined to the particle surface with a volume nearly $10^4$× smaller than the diffraction limit.

In addition to the enhanced excitation rate, also the decay rates of the fluorophore are modified around the particle, resulting in a modified quantum yield. We quantify the emission enhancement as $\xi_{em} = \frac{\phi}{\phi_0}$, which was calculated for a single-wavelength dipole emitting at 730 nm (Stokes shifted by 25 nm from the excitation) and was orientation averaged (see Supporting Information). Note here that we assume the dipole has rotational correlation times shorter than the fluorescence lifetime and that the dipole orientation is fast tumbling within a fluorescent decay (see the influence of a slowly tumbling molecule in Figure S3). In Figure 2c we show $\xi_{em}$ for $\phi_0$ = 1%. The emission enhancement depends strongly on the molecule−surface separation and exhibits a maximum value of 28 at a distance of 4 nm along the center axis of the nanorod. The significant increase in quantum yield especially for positions around the tips of the nanorod is due to the enhancement of the radiative decay rate due to coupling of the dipole emission to the dipolar plasmon of the nanorod. The drastic decrease of the quantum yield at a distance less than 4 nm is attributed to enhanced nonradiative decay through higher order plasmon modes,[47] which accounts for quenching by the nearby particle. Usually single-molecule enzyme studies are performed with higher quantum yield dyes, for which we show the enhancement factors for $\phi_0$ = 25% in Figure 2d. We find a maximum $\xi_{em}$ of only 2 at a distance of 15 nm from the surface because of the already high $\phi_0$, here the excited-state decay is limited by the radiation efficiency of plasmons.[47] Note here that the distance of maximum quantum yield enhancement is different for dyes with different intrinsic quantum yield. This is due to the fact that the enhancement of the nonradiative rate decays faster with separation than the radiative rate enhancement, resulting in a maximal quantum yield enhancement at a certain distance from the surface that depends on the intrinsic quantum yield. The total fluorescence enhancement $\xi_{EF}$ is then a combination of excitation enhancement and emission enhancement, given by

$$\xi_{EF} = \xi_{exc}\xi_{em} \tag{7}$$

This total fluorescence enhancement $\xi_{EF}$ is shown in Figure 2e,f, again for two values of the intrinsic quantum yield. For $\phi_0$ = 1%, the maximum $\xi_{EF}$ is as high as 20000 at a distance of 2.5 nm from the tip, whereas for $\phi_0$ = 25%, $\xi_{EF}$ decreases to a maximum of 1000 at a distance of 2.8 nm. These results imply that the majority of the enhancement is due to excitation enhancement, whereas the emission enhancement is significant only for fluorophores with a low $\phi_0$. The positions with maximum fluorescence enhancement will be used as the exact location of the enzyme active site, which is the starting point of the Brownian motion trajectories.

In addition to enhancement of the excitation rate and quantum yield, also the saturation intensity $I_{sat}$ is modified in the presence of a plasmonic particle.[43] Since higher $I_{sat}$ directly leads to higher photon emission rates, an increased $I_{sat}$ is beneficial to the detection of a fluorescent product. Experimentally 50-fold higher photon count rate has been reported, combined with a 10-fold higher total photon count.[43]



DOI: 10.1021/acsphotonics.8b00327
ACS Photonics 2018, 5, 3073−3081

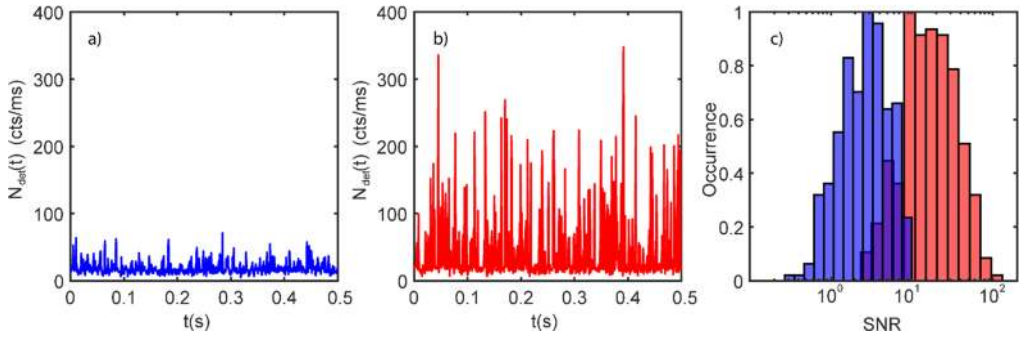


**Figure 4.** Simulated time traces of single enzyme turnovers. The number of detected photons $N_{det}(t)$ with shot-noise superposed, without (a) and with (b) a AuNR, and (c) the histogram showing the SNR distribution evaluated from the time traces shown in (a) and (b). Simulation is based on an 82 × 30 nm$^2$ AuNR, which is under 705 nm laser excitation, with $I_0 = 2 \times 10^9$ W m$^{-2}$. For both simulations we used $t_{int} = 1$ ms and $\phi_0 = 25\%$.

In our calculation, where $I_{sat} = \frac{\gamma_{tot} h\nu}{2\sigma_{abs}}$, the increase of saturation level is determined by the modification of distance-dependent total decay rate $\gamma_{tot}$ and is found to be 3 orders of magnitude enhanced on the particle surface, and decreases rapidly within 10 nm.

To quantify the effect of plasmon-enhancement, we consider the enzyme reaction in the presence and absence of the plasmonic particle. In Figure 3a we show a typical trajectory of a single fluorophore diffusing away from the center of a Gaussian focus, and Figure 3b shows the time-dependent PCR($\tau$)of a single turnover event according to eq 6. The residence time in the confocal volume varies from 100 $\mu$s to 1 ms for individual fluorophores due to the random nature of the trajectories. In Figure 3c,d we show the trajectory and the plasmon-enhanced photon counts for a fluorophore ($\phi_0$ = 25%) starting at 2.8 nm from the tip of a 82 × 30 nm$^2$ nanorod in a 3D Gaussian excitation beam. The plasmon-enhanced time trace shows a 1000-fold enhancement in maximum photon detection rate compared to the confocal-only case, in agreement with Figure 2. Although the intensity is enhanced 1000-fold, the fluorophore spends on average 100× shorter in the near-field compared to a confocal volume.

In Figure 4a,b we show the comparison of the simulated time trace of single enzyme turnovers without and with plasmonic particle respectively for $t_{int}$ = 1 ms. Despite this much shorter residence time, the plasmon enhancement wins and we find a significant enhancement in$N_{det}(t)$ for experimentally relevant binning times of $t_{int}$ = 1 ms. For the confocal excitation, we used the SNR reported in previous experimental results as a benchmark, and by varying the autohydrolyzed fraction $f_h$ in eq 5 and collection efficiency $\eta_{col}$ in eq 6, we find an average SNR = 3 for $I_0 = 2 \times 10^9$ W m$^{-2}$ that closely resembles literature reports.[7,14] This indicates that our simulation generates the correct signal and background intensities. As can be seen, the plasmon-enhanced time trace (b) exhibits a significantly higher SNR where all events are clearly visible above the background.

In Figure 4c we show the histogram of the SNR of each event, which shows a 7-fold increase in average SNR due to plasmon enhancement. More importantly, in the plasmon-enhanced time trace, all simulated events exhibit SNR > 1, whereas ∼30% of events exhibit SNR < 1 for confocal-only excitation. This is crucial for single enzyme measurements because a high SNR will significantly increase the accuracy of waiting time determination and will alleviate the uncertainties now experienced in various threshold-finding algorithms.[14]

We show in Figure 5 the SNR with (red curve) and without (blue curve) plasmon enhancement, as a function of incident

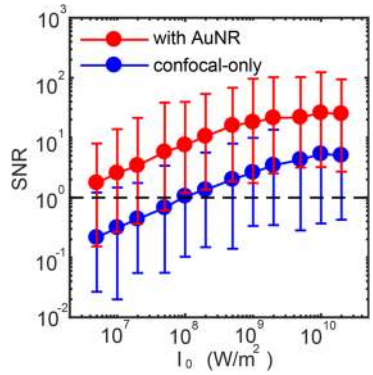


**Figure 5.** SNR in single enzyme turnover detection as a function of laser intensity.The simulation is based on an 82 × 30 nm$^2$ AuNR, with 705 nm laser excitation, $t_{int}$ = 1 ms, and $\phi_0$ = 25%.

laser intensity$I_0$. We evaluate the SNR under 705 nm laser intensity $I_0$ from 5 × 10$^6$ to 2 × 10$^{10}$ W m$^{-2}$ corresponding to incident laser powers of 1 $\mu$W to 2 mW focused by an objective lens with NA = 1.2. The errors bars indicate the full width of the distribution of SNR per event, which spans 1−2 decades due to the broadly distributed residence time of diffusing fluorophores caused by Brownian motion.

For the confocal-only simulations, we find an average SNR > 1 for $I_0 > 2 \times 10^8$ W m$^{-2}$, and the SNR does not increase anymore beyond $I_0 = 5 \times 10^9$ W m$^{-2}$ due to fluorescence saturation (see eq 4). This results in a maximum average SNR in confocal-only simulations of ∼4. With plasmon enhancement we show that the SNR can be enhanced by more than an order of magnitude under these conditions. The increase in SNR under plasmon enhancement is attributed to the strong fluorescence enhancement around the gold nanorod, implying that although the residence time is shorter by ∼100×, a significant increase in PCR($\tau$) is still expected due to fluorescence enhancement. However, although the saturation level of fluorophores close to the particle is increased due to strong increase of $\gamma_{tot}$, the SNR still saturates at a value of ∼25 due to the increased (but still limited) saturation intensity.

The structure and activity of proteins can be impaired when they are heated at a certain temperature for extended periods of time. From heat conduction calculations we estimate the surface temperature rise and find that for $I_0 = 1 \times 10^8$ W m$^{-2}$, the average temperature rise is 19 K (see Supporting



DOI: 10.1021/acsphotonics.8b00327
ACS Photonics 2018, 5, 3073−3081

Information, Figure S1), well below the denaturing point of many enzymes.[48] In the remainder of our calculations we therefore use $I_0 = 1 \times 10^8$ W m$^{-2}$.

The overall enhancement is a trade-off between fluorescence enhancement and the residence time of the fluorophore in the near-field. The latter depends on the size of the particle, which is illustrated in Figure 6a. There we show averaged and

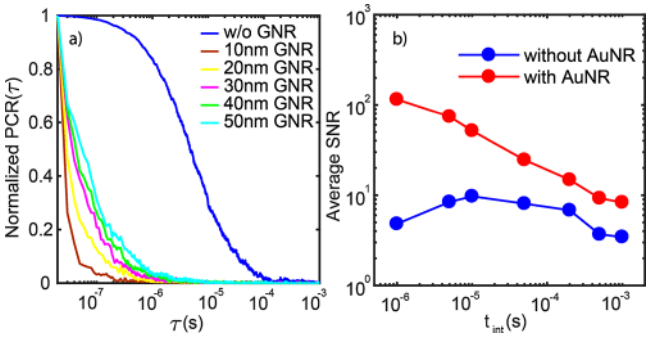


**Figure 6.** (a) Normalized PCR time traces of single fluorophores diffusing away from the active site of an enzyme coupled to a AuNR with different widths. Time traces are averaged over ~400 trajectories. The particles have a fixed plasmon wavelength $\lambda_{sp}$ = 705 nm. (b) Average SNR as a function of binning time $t_{int}$ for a nanorod with a width of 30 nm and the confocal-only case. The excitation wavelength is 705 nm with $I_0 = 1 \times 10^8$ W m$^{-2}$ and $\phi_0$ = 25% for all calculations to facilitate comparison. In order to keep $\lambda_{sp}$ = 705 nm for all particles the aspect ratios vary slightly.

normalized time traces of single fluorophores generated by the enzyme in the absence and presence of a particle, averaged over ~400 events. For the confocal-only case we observe an average residence time of ~10 $\mu$s, whereas the residence time in the near-field of a nanorod is typically >100× shorter. As expected, we find that the residence time increases with nanoparticle width, a direct consequence of the greater extent of the near-field for larger particles.

The short residence times we find in Figure 6a imply that the SNR will depend strongly on the binning time used in the experiments. This effect is shown in Figure 6b, where we compare the confocal-only case with a 30 nm wide nanorod. For all evaluated binning times $t_{int}$ the average SNR is significantly increased (by a factor of 10 × 100) due to plasmon enhancement. For the confocal-only case, we find an optimum binning time of about 10 $\mu$s, which matches with the average residence time of the product in the laser focus. For shorter integration time, not all signal is collected within one integration time, resulting in a lower SNR of the bursts. In the presence of a 30 nm wide nanorod we find that the SNR increases monotonously with decreasing binning time, with 100-fold enhancement compared to the confocal SNR for $t_{int}$ = 1 $\mu$s. Again we expect an optimum in the SNR when $t_{int}$ matches the residence time in the near-field, but this now occurs for $t_{int}$ < 1 $\mu$s, which is difficult to access experimentally. For experimentally feasible binning times of 100 $\mu$s we find that the SNR in the presence of a 30 nm wide particle is approximately enhanced 5× compared to the confocal-only case.

In Figure 7a, we show the SNR as a function of particle width. To compare between different plasmonic materials, we also calculate the SNR enhancement for silver nanorods (AgNRs). As expected we find that the SNR enhancement

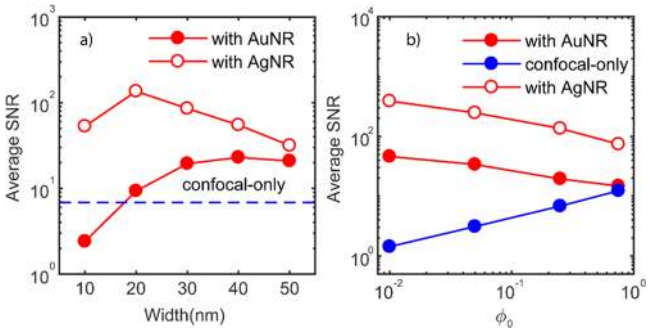


**Figure 7.** (a) SNR as a function of the width of the particle for both gold and silver nanorods with $\lambda_{SP}$ = 705 nm, the dotted blue line indicates the confocal-only SNR. Simulation parameters: $I_0 = 2 \times 10^9$ W m$^{-2}$ for confocal-only and $I_0 = 1 \times 10^8$ W m$^{-2}$ for the plasmon-enhanced case, $\phi_0$ = 25%, and $t_{int}$ = 100 $\mu$s. Note that the calculations for confocal-only were performed with a higher power density than the enzyme-nanoparticle conjugates, see the text for further details. (b) Dependence of the average SNR on $\phi_0$ for particles with $\lambda_{SP}$ = 705 nm. The AuNR has size 82 × 30 nm$^2$, the AgNR is 72 × 20 nm$^2$.

with AgNRs is higher than AuNRs by a factor up to 10, caused by a reduced absorption by the bulk metal which results in a higher local field enhancement and dipolar radiation efficiency (see Figure S5 in Supporting Information). For widths from 10 to 20 nm the SNR increases for both AuNRs and AgNRs, which is the result of an increased residence time in the near-field combined with a higher emission enhancement for larger particles. For increasing widths radiation damping causes broadening of the plasmon resonance[49] and concurrent reduction in fluorescence enhancement.[50] For AgNRs, significant radiation damping starts for ~20 nm width, while for AuNRs this onset is shifted to widths of 30−40 nm (see Figure S6 in Supporting Information) This implies that for AuNRs, even though emission enhancement is stronger for larger particles, this effect is similar in magnitude as the reduced excitation enhancement due to radiation damping. The result is a SNR that does not strongly depend on particle size for particles with a width larger than 30 nm. For AgNRs, the stronger radiation damping for larger particles results in a decreasing SNR for particles with a width larger than 20 nm. This trade-off between emission enhancement and radiation damping results in an optimum particle size that is different for gold versus silver due to a different onset of radiation damping.

It is known that fluorophores with a low intrinsic quantum yield are enhanced more by coupling to the plasmon.[47] We therefore also investigate the influence of $\phi_0$on the average SNR, see Figure 7b. For the confocal-only case, we observe an increasing SNR with $\phi_0$simply due to the fact that more signal is generated for a higher $\phi_0$. The SNR scales approximately with the square-root of $\phi_0$, as expected for shot-noise limited detection with low (but here nonzero) background. However, due to the strong decrease of fluorescence enhancement as a function of $\phi_0$, the plasmon-enhanced SNR decreases with $\phi_0$ (see Supporting Information, Figure S7). In addition, lowering $\phi_0$ reduces the background due to autohydrolyzed substrate, resulting in optimum SNR for low $\phi_0$. This implies that simply by lowering $\phi_0$ (by, e.g., using quenchers such as methyl viologen[51]) one can improve the SNR in single-molecule enzymology further by a factor of 2−3.

Our results indicate that the maximum experimentally feasible enhancement for AuNRs is ~100× when a fluorogenic substrate with low $\phi_0$ is used in combination with 30 nm wide


DOI: 10.1021/acsphotonics.8b00327
ACS Photonics 2018, 5, 3073−3081

particles. For silver particles, the enhancement is increased to 300× for 20 nm particles. Note that we assumed here that the fluorescent product immediately dissociates from the enzyme. In reality a finite dissociation constant will be associated with the enzyme−product interaction,[14] which results in the product remaining bound for a short time. This will further increase the SNR due to the longer residence time in the near-field of the particle. The enhanced SNR provided by coupling to a plasmonic particle will aid in the quantification of the kinetic heterogeneity of enzymes by allowing for more reliable thresholding and burst-detection.[14] Moreover, it may allow for the first direct measurement of the enzyme−product dissociation process by relating the measured enhancement factor to the residence time of the product in the near-field of the particle. In addition, it has been reported that the enzymatic activity and long-term stability are modified for nanoparticle-bound enzymes.[52] Our method may therefore allow for the quantification of the interfacial activation of enzymes and the elucidation of the underlying mechanisms at the single-molecule level.

## CONCLUSIONS

In conclusion, we studied plasmon-enhanced single-molecule enzymology by combining Brownian dynamics and electromagnetic simulations. We find dramatically enhanced average SNR caused by the enhancement of the fluorescence intensity of a product near a plasmonic nanorod. We show that, although the average residence time is greatly reduced compared to a confocal-only excitation, the SNR can still be largely improved, and a 100−300-fold increase in average SNR has been found for a low quantum yield fluorophore with a binning time of 100 $\mu$s. These enhancements are achieved for enzymes conjugated to the tip of a particle, which can be experimentally achieved using recently reported tip-specific functionalization protocols.[53,54] Our results provide a practical guideline for choosing the optimum particle size and experimental parameters such as intrinsic quantum yield, excitation power, and binning time. The increase in SNR has important implications in the study of single-molecule enzymology, since we show that in the presence of a plasmonic nanoparticle all bursts exhibit SNR > 1, which may tremendously help the data analysis in single enzyme kinetics measurement. This may aid in further quantification and understanding of dynamic and static heterogeneity.

## ASSOCIATED CONTENT

### Supporting Information

The Supporting Information is available free of charge on the ACS Publications website at DOI: 10.1021/acsphotonics.8b00327.

(1) Focal field approximations; (2) Estimated particle temperature and implications for protein stability; (3) Derivation of single-molecule photon count rate (PCR) and signal-to-noise ratio (SNR); (4) plasmon-enhanced fluorescence calculations; (5) Brownian motion simulations; (6) Effect of particle size and material on the excitation and emission enhancement; (7) Effect of intrinsic quantum yield on total fluorescence enhancement (PDF).

## AUTHOR INFORMATION


### Corresponding Author

*E-mail: p.zijlstra@tue.nl.

### ORCID

Peter Zijlstra: 0000-0001-9804-2265


### Notes

The authors declare no competing financial interest.

## ACKNOWLEDGMENTS

P.Z. and Y.W. acknowledge financial support from The Netherlands Organization for Scientific Research (NWO VIDI).

## REFERENCES


(1) Schomburg, I.; Chang, A.; Placzek, S.; Söhngen, C.; Rother, M.; Lang, M.; Munaretto, C.; Ulas, S.; Stelzer, M.; Grote, A.; et al. BRENDA in 2013: Integrated Reactions, Kinetic Data, Enzyme Function Data, Improved Disease Classification: New Options and Contents in BRENDA. *Nucleic Acids Res.* **2012**, *41* (D1), D764−D772.

(2) Michaelis, L.; Menten, M. M. L. The Kinetics of Invertin Action. *FEBS Lett.* **2013**, *587* (17), 2712−2720.

(3) Lee, A. I.; Brody, J. P. Single-Molecule Enzymology of Chymotrypsin Using Water-in-Oil Emulsion. *Biophys. J.* **2005**, *88* (6), 4303−4311.

(4) Rondelez, Y.; Tresset, G.; Tabata, K. V.; Arata, H.; Fujita, H.; Takeuchi, S.; Noji, H. Microfabricated Arrays of Femtoliter Chambers Allow Single Molecule Enzymology. *Nat. Biotechnol.* **2005**, *23* (3), 361−365.

(5) Lu, H. P.; Xun, L.; Xie, X. S. Single-Molecule Enzymatic Dynamics. *Science* **1998**, *282* (5395), 1877−1882.

(6) Flomenbom, O.; Velonia, K.; Loos, D.; Masuo, S.; Cotlet, M.; Engelborghs, Y.; Hofkens, J.; Rowan, A. E.; Nolte, R. J.; Van der Auweraer, M.; et al. Stretched Exponential Decay and Correlations in the Catalytic Activity of Fluctuating Single Lipase Molecules. *Proc. Natl. Acad. Sci. U. S. A.* **2005**, *102* (7), 2368−2372.

(7) English, B. P.; Min, W.; van Oijen, A. M.; Lee, K. T.; Luo, G.; Sun, H.; Cherayil, B. J.; Kou, S. C.; Xie, X. S. Ever-Fluctuating Single Enzyme Molecules: Michaelis-Menten Equation Revisited. *Nat. Chem. Biol.* **2006**, *2* (2), 87−94.

(8) De Cremer, G.; Roeffaers, M. B. J.; Baruah, M.; Sliwa, M.; Sels, B. F.; Hofkens, J.; De Vos, D. E. Dynamic Disorder and Stepwise Deactivation in a Chymotrypsin Catalyzed Hydrolysis Reaction. *J. Am. Chem. Soc.* **2007**, *129* (50), 15458−15459.

(9) Rocco, A.; Kierzek, A. M.; McFadden, J. Slow Protein Fluctuations Explain the Emergence of Growth Phenotypes and Persistence in Clonal Bacterial Populations. *PLoS One* **2013**, *8* (1), e54272.

(10) Chen, Q.; Groote, R.; Schönherr, H.; Vancso, G. J. Probing Single Enzyme Kinetics in Real-Time. *Chem. Soc. Rev.* **2009**, *38* (9), 2671−2683.

(11) Velonia, K.; Flomenbom, O.; Loos, D.; Masuo, S.; Cotlet, M.; Engelborghs, Y.; Hofkens, J.; Rowan, A. E.; Klafter, J.; Nolte, R. J. M.; et al. Single-Enzyme Kinetics of CALB-Catalyzed Hydrolysis. *Angew. Chem., Int. Ed.* **2005**, *44* (4), 560−564.

(12) van Oijen, A. M.; Blainey, P. C.; Crampton, D. J.; Richardson, C. C.; Ellenberger, T.; Xie, X. S. Single-Molecule Kinetics of $\lambda$ Exonuclease Reveal Base Dependence and Dynamic Disorder. *Science* **2003**, *301* (5637), 1235−1238.

(13) Terentyeva, T. G.; Hofkens, J.; Komatsuzaki, T.; Blank, K.; Li, C.-B. Time-Resolved Single Molecule Fluorescence Spectroscopy of an $\alpha$-Chymotrypsin Catalyzed Reaction. *J. Phys. Chem. B* **2013**, *117* (5), 1252−1260.

(14) Terentyeva, T. G.; Engelkamp, H.; Rowan, A. E.; Komatsuzaki, T.; Hofkens, J.; Li, C.-B.; Blank, K. Dynamic Disorder in Single-Enzyme Experiments: Facts and Artifacts. *ACS Nano* **2012**, *6* (1), 346−354.




DOI: 10.1021/acsphotonics.8b00327
*ACS Photonics* 2018, 5, 3073−3081

(15) Blank, K.; De Cremer, G.; Hofkens, J. Fluorescence-Based Analysis of Enzymes at the Single-Molecule Level. *Biotechnol. J.* **2009**, *4* (4), 465−479.
(16) Turunen, P.; Rowan, A. E.; Blank, K. Single-Enzyme Kinetics with Fluorogenic Substrates: Lessons Learnt and Future Directions. *FEBS Lett.* **2014**, *588* (19), 3553−3563.
(17) Qian, H.; Kou, S. C. Statistics and Related Topics in Single-Molecule Biophysics. *Annu. Rev. Stat. Its Appl.* **2014**, *1* (1), 465−492.
(18) Moffitt, J. R.; Bustamante, C. Extracting Signal from Noise: Kinetic Mechanisms from a Michaelis−Menten-like Expression for Enzymatic Fluctuations. *FEBS J.* **2014**, *281* (2), 498−517.
(19) Colomb, W.; Sarkar, S. K. Extracting Physics of Life at the Molecular Level: A Review of Single-Molecule Data Analyses. *Phys. Life Rev.* **2015**, *13*, 107−137.
(20) Levene, M. J.; Korlach, J.; Turner, S. W.; Foquet, M.; Craighead, H. G.; Webb, W. W. Zero-Mode Waveguides for Single-Molecule Analysis at High Concentrations. *Science* **2003**, *299* (5607), 682−686.
(21) Punj, D.; Ghenuche, P.; Moparthi, S. B.; de Torres, J.; Grigoriev, V.; Rigneault, H.; Wenger, J. Plasmonic Antennas and Zero-Mode Waveguides to Enhance Single Molecule Fluorescence Detection and Fluorescence Correlation Spectroscopy toward Physiological Concentrations. *Wiley Interdiscip. Rev. Nanomed. Nanobiotechnol.* **2014**, *6* (3), 268−282.
(22) Gérard, D.; Wenger, J.; Bonod, N.; Popov, E.; Rigneault, H.; Mahdavi, F.; Blair, S.; Dintinger, J.; Ebbesen, T. W. Nanoaperture-Enhanced Fluorescence: Towards Higher Detection Rates with Plasmonic Metals. *Phys. Rev. B: Condens. Matter Mater. Phys.* **2008**, *77* (4), 045413.
(23) Wenger, J.; Gérard, D.; Dintinger, J.; Mahboub, O.; Bonod, N.; Popov, E.; Ebbesen, T. W.; Rigneault, H. Emission and Excitation Contributions to Enhanced Single Molecule Fluorescence by Gold Nanometric Apertures. *Opt. Express* **2008**, *16* (5), 3008−3020.
(24) Giannini, V.; Fernández-Domínguez, A. I.; Heck, S. C.; Maier, S. A. Plasmonic Nanoantennas: Fundamentals and Their Use in Controlling the Radiative Properties of Nanoemitters. *Chem. Rev.* **2011**, *111* (6), 3888−3912.
(25) Taylor, A. B.; Zijlstra, P. Single-Molecule Plasmon Sensing: Current Status and Future Prospects. *ACS Sens.* **2017**, *2* (8), 1103−1122.
(26) Gersten, J.; Nitzan, A. Spectroscopic Properties of Molecules Interacting with Small Dielectric Particles. *J. Chem. Phys.* **1981**, *75* (3), 1139−1152.
(27) Gersten, J. I. Theory of Fluorophore-Metallic Surface Interactions. *Radiative Decay Engineering; Topics in Fluorescence Spectroscopy*; Springer: Boston, MA, 2005; pp 197−221.
(28) Tam, F.; Goodrich, G. P.; Johnson, B. R.; Halas, N. J. Plasmonic Enhancement of Molecular Fluorescence. *Nano Lett.* **2007**, *7* (2), 496−501.
(29) Koenderink, A. F. Single-Photon Nanoantennas. *ACS Photonics* **2017**, *4* (4), 710−722.
(30) Yuan, H.; Khatua, S.; Zijlstra, P.; Yorulmaz, M.; Orrit, M. Thousand-Fold Enhancement of Single-Molecule Fluorescence Near a Single Gold Nanorod. *Angew. Chem., Int. Ed.* **2013**, *52* (4), 1217−1221.
(31) Khatua, S.; Paulo, P. M. R.; Yuan, H.; Gupta, A.; Zijlstra, P.; Orrit, M. Resonant Plasmonic Enhancement of Single-Molecule Fluorescence by Individual Gold Nanorods. *ACS Nano* **2014**, *8* (5), 4440−4449.
(32) Akselrod, G. M.; Argyropoulos, C.; Hoang, T. B.; Ciracì, C.; Fang, C.; Huang, J.; Smith, D. R.; Mikkelsen, M. H. Probing the Mechanisms of Large Purcell Enhancement in Plasmonic Nanoantennas. Nat. *Nat. Photonics* **2014**, *8* (11), 835−840.
(33) Flauraud, V.; Regmi, R.; Winkler, P. M.; Alexander, D. T. L.; Rigneault, H.; van Hulst, N. F.; García-Parajo, M. F.; Wenger, J.; Brugger, J. In-Plane Plasmonic Antenna Arrays with Surface Nanogaps for Giant Fluorescence Enhancement. *Nano Lett.* **2017**, *17* (3), 1703−1710.
(34) Acuna, G. P.; Moller, F. M.; Holzmeister, P.; Beater, S.; Lalkens, B.; Tinnefeld, P. Fluorescence Enhancement at Docking Sites of DNA-Directed Self-Assembled Nanoantennas. *Science* **2012**, *338* (6106), 506−510.
(35) Puchkova, A.; Vietz, C.; Pibiri, E.; Wünsch, B.; Sanz Paz, M.; Acuna, G. P.; Tinnefeld, P. DNA Origami Nanoantennas with over 5000-Fold Fluorescence Enhancement and Single-Molecule Detection at 25 MM. *Nano Lett.* **2015**, *15* (12), 8354−8359.
(36) Punj, D.; Regmi, R.; Devilez, A.; Plauchu, R.; Moparthi, S. B.; Stout, B.; Bonod, N.; Rigneault, H.; Wenger, J. Self-Assembled Nanoparticle Dimer Antennas for Plasmonic-Enhanced Single-Molecule Fluorescence Detection at Micromolar Concentrations. *ACS Photonics* **2015**, *2* (8), 1099−1107.
(37) Langguth, L.; Femius Koenderink, A. Simple Model for Plasmon Enhanced Fluorescence Correlation Spectroscopy. Opt. *Opt. Express* **2014**, *22* (13), 15397−15409.
(38) Langguth, L.; Osorio, C. I.; Koenderink, A. F. Exact Analysis of Nanoantenna Enhanced Fluorescence Correlation Spectroscopy at a Mie Sphere. *J. Phys. Chem. C* **2016**, *120* (25), 13684−13692.
(39) Punj, D.; Mivelle, M.; Moparthi, S. B.; van Zanten, T. S.; Rigneault, H.; van Hulst, N. F.; García-Parajó, M. F.; Wenger, J. A Plasmonic 'Antenna-in-Box' Platform for Enhanced Single-Molecule Analysis at Micromolar Concentrations. *Nat. Nanotechnol.* **2013**, *8* (7), 512−516.
(40) Wenger, J. Fluorescence Enhancement Factors on Optical Antennas: Enlarging the Experimental Values without Changing the Antenna Design. *Int. J. Opt.* **2012**, *2012*, 1.
(41) Khatua, S.; Yuan, H.; Orrit, M. Enhanced-Fluorescence Correlation Spectroscopy at Micro-Molar Dye Concentration around a Single Gold Nanorod. *Phys. Chem. Chem. Phys.* **2015**, *17* (33), 21127−21132.
(42) Pradhan, B.; Khatua, S.; Gupta, A.; Aartsma, T.; Canters, G.; Orrit, M. Gold-Nanorod-Enhanced Fluorescence Correlation Spectroscopy of Fluorophores with High Quantum Yield in Lipid Bilayers. *J. Phys. Chem. C* **2016**, *120* (45), 25996−26003.
(43) Wientjes, E.; Renger, J.; Cogdell, R.; van Hulst, N. F. Pushing the Photon Limit: Nanoantennas Increase Maximal Photon Stream and Total Photon Number. *J. Phys. Chem. Lett.* **2016**, *7* (9), 1604−1609.
(44) Regmi, R.; Winkler, P. M.; Flauraud, V.; Borgman, K. J. E.; Manzo, C.; Brugger, J.; Rigneault, H.; Wenger, J.; García-Parajo, M. F. Planar Optical Nanoantennas Resolve Cholesterol-Dependent Nanoscale Heterogeneities in the Plasma Membrane of Living Cells. *Nano Lett.* **2017**, *17* (10), 6295−6302.
(45) Lohse, S. E.; Murphy, C. J. The Quest for Shape Control: A History of Gold Nanorod Synthesis. *Chem. Mater.* **2013**, *25* (8), 1250−1261.
(46) http://brenda-enzymes.org/index.php (accessed Dec 19, 2017).
(47) Mertens, H.; Polman, A. Strong Luminescence Quantum-Efficiency Enhancement near Prolate Metal Nanoparticles: Dipolar versus Higher-Order Modes. *J. Appl. Phys.* **2009**, *105* (4), 044302.
(48) Robertson, A. D.; Murphy, K. P. Protein Structure and the Energetics of Protein Stability. *Chem. Rev.* **1997**, *97* (5), 1251−1268.
(49) Sönnichsen, C.; Franzl, T.; Wilk, T.; von Plessen, G.; Feldmann, J.; Wilson, O.; Mulvaney, P. Drastic Reduction of Plasmon Damping in Gold Nanorods. *Phys. Rev. Lett.* **2002**, *88* (7), 077402.
(50) Guzatov, D. V.; Vaschenko, S. V.; Stankevich, V. V.; Lunevich, A. Y.; Glukhov, Y. F.; Gaponenko, S. V. Plasmonic Enhancement of Molecular Fluorescence near Silver Nanoparticles: Theory, Modeling, and Experiment. *J. Phys. Chem. C* **2012**, *116* (19), 10723−10733.
(51) Ha, T.; Tinnefeld, P. Photophysics of Fluorescent Probes for Single-Molecule Biophysics and Super-Resolution Imaging. *Annu. Rev. Phys. Chem.* **2012**, *63* (1), 595−617.
(52) Vranish, J. N.; Ancona, M. G.; Walper, S. A.; Medintz, I. L. Pursuing the Promise of Enzymatic Enhancement with Nanoparticle Assemblies. *Langmuir* **2018**, *34* (9), 2901−2925.
(53) Paulo, P. M. R.; Zijlstra, P.; Orrit, M.; Garcia-Fernandez, E.; Pace, T. C. S.; Viana, A. S.; Costa, S. M. B. Tip-Specific Functionalization of Gold Nanorods for Plasmonic Biosensing: Effect of Linker Chain Length. *Langmuir* **2017**, *33* (26), 6503−6510.


DOI: 10.1021/acsphotonics.8b00327
*ACS Photonics* 2018, 5, 3073−3081

(54) Caswell, K. K.; Wilson, J. N.; Bunz, U. H. F.; Murphy, C. J. Preferential End-to-End Assembly of Gold Nanorods by Biotin–Streptavidin Connectors. *J. Am. Chem. Soc.* **2003**, *125* (46), 13914–13915.



DOI: 10.1021/acsphotonics.8b00327
*ACS Photonics* 2018, 5, 3073–3081